2012

Non-Isothermal Cool Flames in Unstirred Static Reactors: A Compressible Model with Global Kinetics

Michael R. Foster
George Fox University, mfoster@georgefox.edu

Howard Pearlman
Drexel University

Non-Isothermal Cool Flames in Unstirred Static Reactors: A Compressible Model with Global Kinetics

Michael R. Foster · Howard Pearlman

Abstract A compressible model is developed with kinetics based on the Wang–Mou five-step global kinetic scheme and used to evaluate the temperature, concentration, and velocity fields characteristic of low-temperature combustion in unstirred static reactors. This work relaxes the assumption of small exothermicity that enabled prior studies to employ the Boussinesq approximation, valid for cases where $\beta\Delta T << 1$, i.e., slow reactions and cool flames. In this study, the range of validity of the model is extended to cases with large temperature excursions, including multi-stage ignition. For the weakly exothermic cases considered, including modes of slow reaction and cool flames, the Boussinesq approximation is completely adequate. However, it overpredicts the density change and underpredicts the ignition delay time for high-temperature ignitions. Qualitative comparison with experimental results acquired at microgravity conditions are also discussed.

Keywords Low-temperature combustion · Cool flames · Compressible model · Wang–Mou model · Critical Rayleigh number

M. R. Foster (✉)
Department of Engineering, George Fox University,
414 N. Meridian St., Box 6141, Newberg, OR 97132, USA
e-mail: mfoster@georgefox.edu

H. Pearlman
Advanced Cooling Technologies, Inc., Lancaster,
PA 17601, USA

Introduction

The heat generated during low and intermediate temperature reactions in unstirred, closed vessels often induces buoyant flows that stir the reaction. These flows are caused by density gradients induced by temperature non-uniformities and have contributed to inconsistencies in unstirred reactor studies sometimes performed in different size and shape vessels. Such complexities were recognized more than forty years ago (Tyler 1966; Fine et al. 1970) and even date back to the development of thermal ignition theory by Semenov (1935) and Frank-Kamenetskii (1955) who clearly recognized the importance of natural convection on ignition (with Frank-Kamenetskii commenting that natural convection was disregarded in the early development of the theory to avoid complexities). Furthermore, the need to suppress buoyant complexities in unstirred hydrocarbon ignition studies performed in the '60's and '70's (Tyler 1966; Fine et al. 1970; Barnard and Harwood 1974) inspired the development of continuously stirred tank reactors (CSTR's). By eliminating spatial variations in the species and temperature distributions within the reactor, CSTR's simplified the need to understand the transport processes in unstirred reactors and became a more useful tool for validating combustion chemistry models.

In recent years, initial efforts to study the coupled effects of diffusion and chemical reaction on low-temperature reactions and cool flames have focused on using unstirred reactors. In part, the renewed interest was inspired by the demonstrated ability to suppress buoyant convection in unstirred reactors by performing experiments at microgravity conditions (Pearlman 2000, 2007; Foster and Pearlman 2006a), which enable

the Rayleigh number to be reduced by several orders of magnitude noting that $Ra = \beta g \Delta T R^3/\nu\alpha$ and thus the Ra scales linearly with g. Other available options for reducing the Ra include: (1) reducing the reactor pressure ($Ra \propto P^2$), (2) adding inert gas dilution to reduce the temperature excursion ($Ra \propto \Delta T$), and (3) reducing the reactor size ($Ra \propto R^3$). Changing the pressure or size of the reactor, however, can change the chemistry that occurs in the reactor and the heat transfer; whereas by changing the gravitational acceleration and the associated buoyant stirring, all reactor parameters can otherwise remain fixed. This was recognized by Barnard and Harwood (1974) who noted that "it is generally assumed that heat losses are purely conductive. While this may be valid for certain low pressure slow combustion regimes, it is unlikely to be true for the cool flame and ignition regimes" in unstirred reactor studies.

Regarding the critical value for onset of convection in unstirred reactor studies, most researchers have taken the $Ra_{cr} = 600$ based on experimental results from Tyler (1966) and Fine et al. (1970), yet in some cases, the critical Ra for onset of convection has even been shown to be as low as 200 (Campbell et al. 2007). At Earth gravity, it is experimentally difficult, if not impossible, to achieve a Ra less than about 600, which is required to suppress convection by even a combination of the variables listed above. Conveniently, however, microgravity studies can achieve Ra's in this range and below and do not require a change in pressure, mixture composition (e.g., inert dilution), or reduction in vessel size. Access to such facilities is however limited and expensive. Ground-based facilities such as parabolic aircraft, which effectively have a gravitational acceleration that is two orders of magnitude smaller than Earth gravity, Ra's on the order of 1000 are achievable. Drop towers offer an opportunity to reduce g by up to six orders of magnitude, yet the available time duration is generally too short to study low-temperature, slow reactions and cool flames.

Regarding cool flame studies, reduced gravity experiments have been performed aboard NASA's KC-135 aircraft at different gravity levels (different Ra's) (Foster and Pearlman 2006a; Foster 2006), and CFD studies that include reaction, diffusion, and convection have been developed using global kinetic schemes. The schemes include the two-step Sal'nikov mechanism (Campbell et al. 2005b, 2006), the Gray-Yang mechanism (Pearlman et al. 2003; Foster and Pearlman 2006a, b; Foster 2006), and the Wang–Mou mechanism (Cardoso et al. 2004a, b; Campbell et al. 2005a, b, 2006; Foster 2007; Pearlman and Foster 2008). In addition, Fairlie et al. (2005) have taken their reduced mechanism for low-temperature propane oxidation added diffusion of species and heat and used it to compute the spatial and temporal evolution of the temperature and species concentration profiles in an unstirred reactor.

In unstirred static reactor studies, transport typically occurs by diffusive fluxes of heat and species and buoyant convection. However, most models either disregard natural convection or assume that the density variations are small enough to justify the use of the Boussinesq approximation. This assumption is appropriate for slow reactions and weakly exothermic cool flames, yet it is not justified for strongly exothermic reactions including multi-stage or single-stage ignition for which $Ra > Ra_{cr}$. For cool flames, the heat release results in temperature excursions on the order of 20–200K, and for ignition events, the temperature rise is on the order of 1000 K. For a typical reaction that occurs at 600 K, for example, $\beta\Delta T$ ranges from $20/600 = 0.03$ to $200/600 = 0.33$ and even larger values for ignitions. As the temperature excursion increases, $\beta\Delta T << 1$ is not satisfied. For these cases, the Boussinesq approximation is not justified and does not accurately capture the change in density, yet a compressible model can more accurately compute natural convection in strongly non-isothermal cases. Therefore, one of the objectives in this paper is to explore the behavior of non-isothermal cool flames and low-temperature ignition modes representative of hydrocarbon oxidation within a compressible framework and evaluate the importance of variable density on the temperature and species distributions and flow field.

While determination of the critical Rayleigh number for onset of convection does not require a compressible model since the density difference is generally small at the onset of convection, compressibility effects become increasingly important as the density changes increase and the resulting convective flows increase in intensity. For example, such instances arise when low temperature reactions transition to ignition (i.e., multi-stage ignition).

The model herein reported is based on the compressible form of the Navier–Stokes equation coupled with species conservation and energy equations. The chemical kinetic model used is the Wang–Mou global kinetic mechanism (Wang and Mou 1985), a global

Table 1 Wang–Mou thermokinetic scheme (Wang and Mou 1985)

(I)	$y \rightarrow x$	Initiating
(II)	$x + y \rightarrow 2x$	High-temperature branching
(III)	$x \rightarrow 2x$	Low-temperature branching
(IV)	$x \rightarrow S_1$	High-temperature termination
(V)	$x \rightarrow S_2$	Low-temperature termination

Table 2 Summary of the Wang–Mou global model (Wang and Mou 1985)

Reaction rate, $\bar{k}_i$ [a]	Pre-exponential factor, $\bar{A}_i$ [b]	Activation energy, $\bar{E}_i$ [J/mol]	Heat release, $\bar{h}_i$ [J/mol]
$\bar{k}_1 = \bar{A}_1 \bar{N}_o \exp\left(-\bar{E}_1/\bar{R}_u\bar{T}\right)$	1.6×10^4	100416	0
$\bar{k}_2 = \bar{A}_2 \exp\left(-\bar{E}_2/\bar{R}_u\bar{T}\right)$	3.7×10^6	104600	384928
$\bar{k}_3 = \bar{A}_3 \bar{N}_o \exp\left(-\bar{E}_3/\bar{R}_u\bar{T}\right)$	1.38×10^2	29288	16736
$\bar{k}_4 = \bar{A}_4 \bar{N}_o \exp\left(-\bar{E}_4/\bar{R}_u\bar{T}\right)$	7.8×10^4	66944	83680
$\bar{k}_5 = \bar{A}_5 \bar{N}_o^{1/2}/(2\bar{R}_o)$	3.3×10^{-2}	0	0

[a] $\bar{k}_{1,3-5}$ [s^{-1}], $\bar{k}_2$ [m^3/(mol s)]
[b] $\bar{A}_{1-4}$ [m^3/(mol s)], $\bar{A}_5$ [$m^{5/2}$/($mol^{1/2}$ s)]

scheme that is based on the Gray–Yang model and shown to capture modes of slow reaction, cool flames, and ignition (Foster 2007; Pearlman and Foster 2008). The mechanism has five-steps that include initiation, high-temperature branching, low-temperature branching, high-temperature termination, and low-temperature termination steps (Wang and Mou 1985; Liang et al. 2003). In the kinetic scheme (shown in Table 1), two lumped species are used and represent the fuel and oxidizer (y) and an autocatalytic chain carrier (x). Also, S_1 and S_2 represent terminal product species.

The governing equations were non-dimensionalized and solved in a spherical domain assuming axisymmetry about the vertical diameter. The Ec defined here is not the traditional Ec, which is a measure of the kinetic energy of the flow to the enthalpy, but rather the ratio shown in Eq. 7 where the flow speed is based on the diffusional velocity. The non-dimensional parameters are listed below where it is noted that dimensional quantities are indicated with a bar.

The reaction rates, $\bar{k}_i$, along with the pre-exponential factors, $\bar{A}_i$; activation energies, $\bar{E}_i$; and associated heat release, $\bar{h}_i$, for each step are taken from Wang and Mou (1985) and summarized in Table 2. The initial gas density, $\bar{N}_o$; universal gas constant, $\bar{R}_u$; and reactor radius, $\bar{R}_o$, are defined along with the other constants in Table 3. In addition, for the purpose of the model, representative property values of the mean molecular weight of the mixture were based on those for the propane/oxygen system, which was the focus of much of the experimental work performed at microgravity. Much work was also performed on equimolar n-butane/oxygen and some of those results are also included for comparative purposes in this study.

Governing Equations

The Compressible Wang–Mou Model

The dimensional form of the continuity, momentum, energy, and species conservation equations can be expressed in the following form:

$$\frac{D\bar{\rho}}{D\bar{t}} = 0 \tag{1}$$

Table 3 Parameters for Wang–Mou models

Constant	Description	Value
$\bar{C}_o$	Initial heat capacity	2007 J/(kg K)
$\bar{D}_Y/\bar{D}_X$	Diffusivity ratio	0.2
$\bar{g}$	Gravity	0.0981 m/s^2
$\bar{\kappa}_{dv}$	Second coefficient of viscosity	$2\bar{\mu}_o/3$ (N · s/m^2)[a]
$\bar{k}_{T,o}$	Thermal conductivity	0.05747 W/(m K)
Le	Lewis number	1
$\bar{M}_{C_3H_8}$	Propane molecular weight	0.044 kg/mol
$\bar{M}_{O_2}$	Oxygen molecular weight	0.032 kg/mol
$\bar{M}_{\text{mix}}$	$0.5\bar{M}_{C_3H_8} + 0.5\bar{M}_{O_2}$ [b]	0.038 kg/mol
$\bar{\mu}_o$	Dynamic viscosity	2.57×10^{-5} kg/(m s)
$\bar{N}_o$	Initial density	$\bar{P}_o/(\bar{R}_u\bar{T}_o)$ (mol/m^3)
$\bar{P}_o$	Initial reactor pressure	case dependent (Pa)
Pr	Prandtl number	1
$\bar{\rho}_o$	Initial reactant density	$\bar{N}_o\bar{M}_{\text{mix}}$ (kg/m^3)
$\bar{\rho}$	Reacting mixture density	$\bar{P}\bar{M}_{\text{mix}}/(\bar{R}_u\bar{T})$
$\bar{R}_o$	Reactor radius	0.015 m
$\bar{R}_u$	Universal gas constant	8.3188 J/(mol K)
$\bar{T}$	Reactor temperature	K
$\bar{T}_o$	Initial reactor temperature	case dependent (K)
$\bar{y}_o$	Initial reactant concentration	$\bar{N}_o/2$ (mol/m^3)

[a] From Stokes Hypothesis
[b] Consistent with experimental results obtained using equimolar fuel-air mixtures reported by Pearlman et al. (2003) and Foster and Pearlman (2007)

$$\bar{\rho}\frac{D\bar{V}}{D\bar{t}} = \bar{\rho}\bar{g} - \bar{\nabla}\bar{P} + \bar{\nabla}\cdot\left[\bar{\mu}_o\left(\frac{\partial\bar{u}_i}{\partial\bar{x}_j}+\frac{\partial\bar{u}_j}{\partial\bar{x}_i}\right)-\left(2\bar{\mu}_o/3-\bar{\kappa}_{dv}\right)(\bar{\nabla}\cdot\bar{V})\bar{\mathrm{I}}\right] \quad (2)$$

$$\bar{\rho}\bar{C}_o\frac{D(\bar{T}-\bar{T}_o)}{D\bar{t}} = \frac{D\bar{P}}{D\bar{t}} + \bar{\nabla}\cdot\left[\bar{k}_{T,o}\bar{\nabla}(\bar{T}-\bar{T}_o)\right] + \bar{\Phi} + \bar{k}_1\bar{h}_1\bar{y} + \left(\bar{k}_2\bar{h}_2\bar{y}+\bar{k}_3\bar{h}_3+\bar{k}_4\bar{h}_4+\bar{k}_5\bar{h}_5\right)\bar{x} \quad (3)$$

$$\frac{D\bar{y}}{D\bar{t}} = \bar{D}_Y\bar{\nabla}^2\bar{y} - \bar{k}_1\bar{y} - \bar{k}_2\bar{x}\bar{y} \quad (4)$$

$$\frac{D\bar{x}}{D\bar{t}} = \bar{D}_X\bar{\nabla}^2\bar{x} + \bar{k}_1\bar{y} + \bar{k}_2\bar{x}\bar{y} + \bar{k}_3\bar{x} - \bar{k}_4\bar{x} - \bar{k}_5\bar{x} \quad (5)$$

where $\bar{\rho}$ is the density (kg/m^3), $\bar{t}$ is the time (s), $\bar{V}$ is the velocity (m/s), and $\bar{\Phi}$ is the dissipation function (W/m^3),

$$\bar{\Phi} = \bar{\mu}_o\left[2\left(\frac{\partial\bar{u}}{\partial\bar{r}}\right)^2 + 2\left(\frac{\partial\bar{v}}{\partial\bar{z}}\right)^2 + \left(\frac{\partial\bar{v}}{\partial\bar{r}}+\frac{\partial\bar{u}}{\partial\bar{z}}\right)^2\right] - \frac{2\bar{\mu}_o}{3}\left(\frac{\partial\bar{u}}{\partial\bar{r}}+\frac{\partial\bar{v}}{\partial\bar{z}}\right)^2 \quad (6)$$

The following non-dimensional groups are then introduced in Eqs. 8–12:

$$R = \frac{\bar{R}}{\bar{R}_o},\ t = \frac{\bar{t}}{\left(\bar{R}_o^2/\bar{D}_Y\right)},\ P = \frac{\bar{P}}{\bar{\mu}_o\bar{D}_Y/\bar{R}_o^2},$$

$$\rho = \frac{\bar{\rho}}{\bar{\rho}_o} = \left(\frac{\bar{\mu}_o\bar{D}_Y}{\bar{R}_o^2\bar{P}_o}\right)\frac{P}{1+\theta},\ \Phi = \frac{\bar{\Phi}}{\bar{\mu}_o\bar{D}_Y^2/\bar{R}_o^4},$$

$$V = \frac{\bar{V}}{\bar{D}_Y/\bar{R}_o},\ Pr = \frac{\bar{\nu}}{\bar{\alpha}},\ Le = \frac{\bar{k}_T}{\bar{\rho}_o\bar{C}_o\bar{D}_Y} = \frac{\bar{\alpha}}{\bar{D}_Y},$$

$$Sc = PrLe = \frac{\bar{\nu}_o}{\bar{D}_Y},\ Ec = \frac{\bar{D}_Y^2}{\bar{C}_o\bar{T}_o\bar{R}_o^2},\ \theta = \frac{(\bar{T}-\bar{T}_o)}{\bar{T}_o},$$

$$Ra = \frac{\bar{\beta}\bar{g}(\Delta\bar{T})\bar{R}_o^3}{\bar{\nu}_o\bar{\alpha}_o},\ k_{j\,(j\neq 2)} = \frac{\bar{k}_j}{\left(\bar{D}_Y/\bar{R}_o^2\right)},$$

$$k_2 = \frac{\bar{k}_2\bar{y}_o}{\left(\bar{D}_Y/\bar{R}_o^2\right)},\ h_j = \frac{\bar{h}_j\bar{y}_o}{\bar{T}_o\bar{\rho}_o\bar{C}_o},\ Y = \frac{\bar{y}}{\bar{y}_o},\ X = \frac{\bar{x}}{\bar{y}_o} \quad (7)$$

where $\bar{P}_o$ is the initial pressure (Pa), $\bar{\nu}_o$ is the kinematic viscosity (m/s^2), $\bar{\alpha}_o$ is the thermal diffusivity (m^2/s), and $\bar{\rho}_o$ is the initial gas density (kg/m^3).

The non-dimensional continuity, energy, and species conservation equations can then be written as:

$$\frac{D\rho}{Dt} = 0 \quad (8)$$

$$\frac{\rho}{Sc}\frac{DV}{Dt} = \left(Le\frac{Ra}{\theta}\right)\rho - \nabla P + \nabla^2 V \quad (9)$$

$$\rho\frac{D\theta}{Dt} = (Sc\ Ec)\frac{DP}{Dt} + Le\nabla^2\theta + (Sc\ Ec)\Phi + \left[k_1h_1Y + (k_2h_2Y + k_3h_3 + k_4h_4 + k_5h_5)X\right] \quad (10)$$

$$\frac{DY}{Dt} = \nabla^2 Y - k_1Y - k_2XY \quad (11)$$

$$\frac{DX}{Dt} = \left(\frac{\bar{D}_X}{\bar{D}_Y}\right)\nabla^2 X + k_1Y + k_2XY + k_3X - k_4X - k_5X \quad (12)$$

The Non-Dimensional Wang–Mou Model Using the Boussinesq Approximation

The compressible model was solved and the results are compared to the reduced form of the model using the Boussinesq approximation (Foster and Pearlman 2006a; Foster 2007; Campbell et al. 2005a, 2007). In the earlier studies, the Boussinesq approximation was used since it is sufficient to gain insight into the effect of natural convection for weak reactions, yet is limited to cases for which $\Delta T/T_o << 1$. As discussed below, this includes slow reactions and most cool flames, yet is not valid for strongly exothermic reactions and ignitions. For reference, the continuity, momentum, and energy equations for the reduced model using the Boussinesq approximation assume the following form (species conservation equations were the same for both models):

$$\bar{\nabla}\cdot\bar{V} = 0 \quad (13)$$

$$\frac{D\bar{V}}{D\bar{t}} = \frac{\bar{\rho}}{\bar{\rho}_o}\bar{g} - \frac{1}{\bar{\rho}_o}\bar{\nabla}\bar{P} + \frac{\bar{\mu}_o}{\bar{\rho}_o}\bar{\nabla}^2\bar{V} \quad (14)$$

$$\bar{\rho}\bar{C}_o\frac{D(\bar{T}-\bar{T}_o)}{D\bar{t}} = \bar{k}_{T,o}\bar{\nabla}^2(\bar{T}-\bar{T}_o) + \bar{k}_1\bar{h}_1\bar{y} + (\bar{k}_2\bar{h}_2\bar{y}+\bar{k}_3\bar{h}_3+\bar{k}_4\bar{h}_4+\bar{k}_5\bar{h}_5)\bar{x} \quad (15)$$

The non-dimensional form of the governing equations can be expressed as:

$$\nabla\cdot V = 0 \quad (16)$$

$$\frac{1}{Sc}\frac{DV}{Dt} = Le\ Ra\left(\frac{1-\theta}{\theta}\right) - \nabla P + \nabla^2 V \tag{17}$$

$$\frac{D\theta}{Dt} = Le\nabla^2\theta + k_1 h_1 Y + \left(k_2 h_2 Y + k_3 h_3 + k_4 h_4 + k_5 h_5\right) X \tag{18}$$

where the Boussinesq approximation is applied through substitution of $(1-\theta)$ for $\bar{\rho}/\bar{\rho}_o$ in the momentum equation (Eq. 14) since $\bar{\rho} \approx \bar{\rho}_o[1 - \bar{\beta}(\bar{T} - \bar{T}_o)]$, such that $\bar{\rho}/\bar{\rho}_o = 1 - (\bar{T} - \bar{T}_o)/\bar{T}_o = 1 - \theta$.

Numerical Method

The coupled species and energy equations were solved in a 2-D axisymmetic half-domain (Fig. 1) of radius $\bar{R}_o$ such that $0 \leq R \leq 1$. The domain was meshed with 4896 triangular elements. Comparing grids with elements of 4896 and 11248 elements, the maximum percent difference for θ at any location was on the order of 10^{-5}. The boundary conditions on the domain for the momentum equation include: along the axis of symmetry, all normal components of velocity = 0; azimuthal symmetry; and no slip on the vessel walls ($V = 0$). For the energy and species equations, the domain also has azimuthal symmetry, no flux of heat or species across the axis of symmetry, a chemically inert boundary at the wall (i.e., $\nabla X = \nabla Y = 0$), and a fixed gas temperature at the wall equal to the initial wall temperature ($\theta = 0$). The initial mixture composition was $\bar{y}_o$, and the initial temperature, velocity, and pressure throughout the domain were $\bar{T} = \bar{T}_o$, $\bar{V} = 0$, and $\bar{P} = \bar{P}_o$, respectively, so that the non-dimensional initial conditions become $Y = 1$, $X = 0$, $\theta = 0$, $V = 0$, and $P = \bar{P}_o \bar{R}_o^2/(\bar{\mu}_o \bar{D}_Y)$. The parent fuel-air mixture was assumed to be equimolar such that $\bar{y}_o = \bar{N}_o/2 = \bar{P}_o/(2\bar{R}_u \bar{T}_o)$.

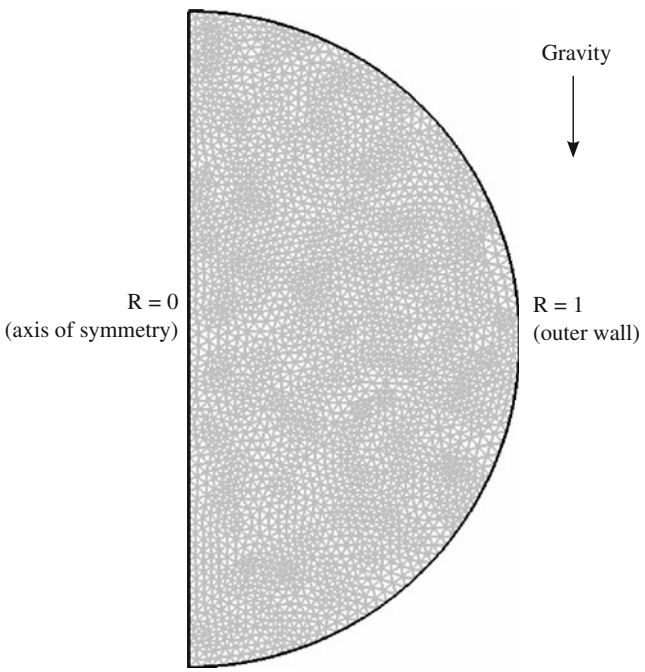

Fig. 1 Meshed domain for 2-D axisymmetric compressible and Boussinesq models

Solutions were obtained using the commercially available COMSOL Multiphysics™ software. The pressure field was discretized using linear Lagrange shape functions; all other variables (fluid velocity, temperature, and concentrations) used quadratic Lagrange shape functions. The nonlinearity arising due to the convective term was handled via damped Newton-Raphson iteration. COMSOL uses an implicit time-dependent solver, IDA (Hindmarsh et al. 2005; COMSOL AB 2008). The integration method in IDA is variable-order, variable-coefficient BDF (between 1 and 5), in fixed-leading-coefficient form. The time-stepping was variable. The relative tolerance on the non-dimensional velocity, pressure, temperature, and species concentrations was 10^{-6}, while the absolute tolerances on each variable were as follows: θ, 1×10^{-7}; u, 1×10^{-4}; v, 1×10^{-4}; Y, 1×10^{-6}; X, 1×10^{-7}; and P, 1×10^{4} except where noted. Increasing or decreasing all the tolerances by an order of magnitude yielded a difference in the computed values of $\theta(t)$, $\rho(t)$, and $Y(t)$ at the center of the reactor of less than 0.5%. The temporal discretization was adapted to attain the combination of relative and absolute tolerances.

Other parameters needed in the model are listed in Table 3. The constant parameter values used to compute the non-dimensional quantities were taken for an equimolar *n*-propane/oxygen premixture at 630 K and 80 kPa.

Experimental Apparatus and Procedures

In the following section, some qualitative comparisons are made between the model predictions and experimental results shown in Fig. 2. For additional information on experimental work, please refer to Foster and Pearlman (2006a) and Foster (2006, 2007). The experiments were obtained at microgravity conditions aboard NASA's KC-135 aircraft. Specifically, static reactor experiments were performed in a closed, 10.2 cm i.d., spherical, fused-silica reaction vessel. The vessel was initially heated to 300–350°C inside of a box furnace.

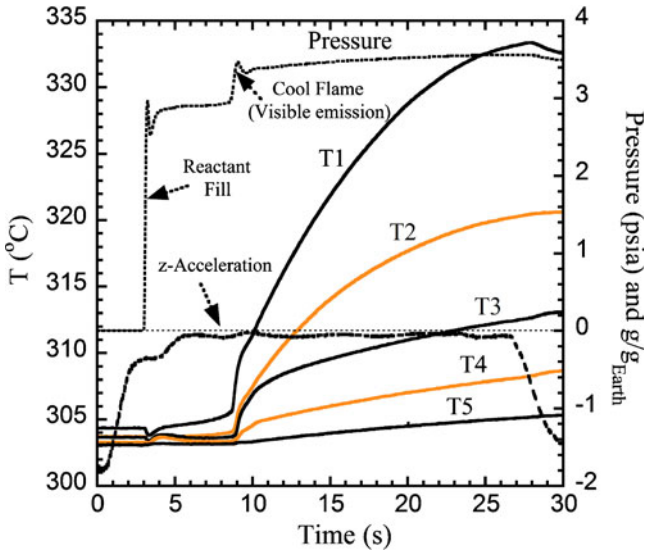

(a) $T = 304°\mathrm{C}$, $P_{initial} = 2.9$ psia

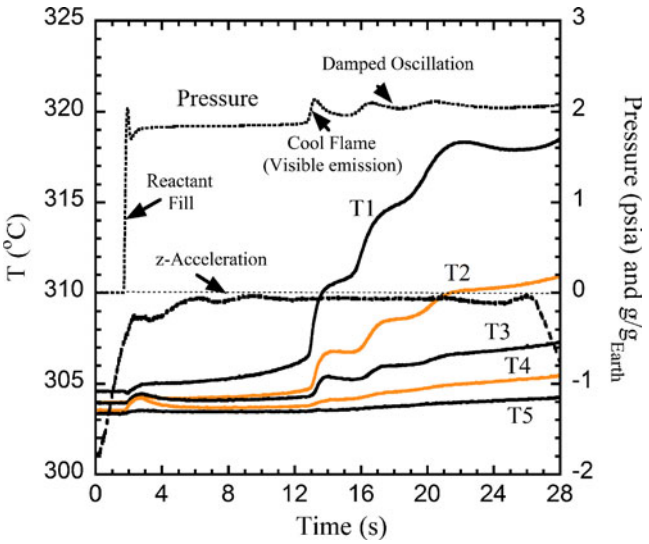

(b) $T = 304°\mathrm{C}$, $P_{initial} = 1.84$ psia

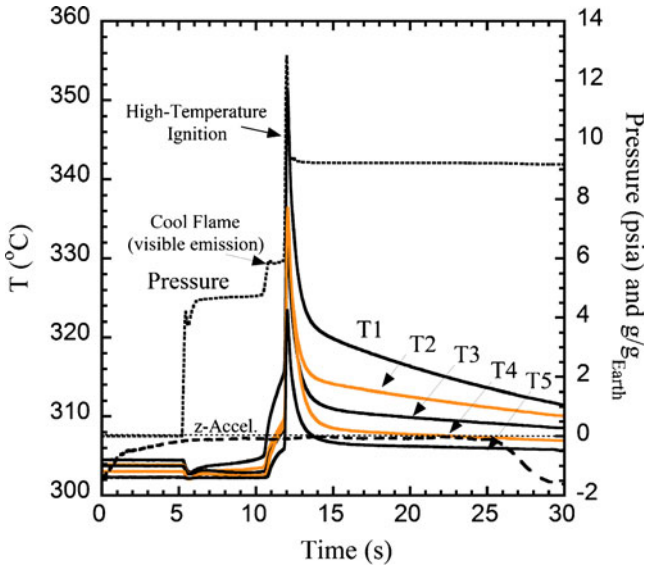

(c) $T = 304°\mathrm{C}$, $P_{initial} = 4.6$ psia

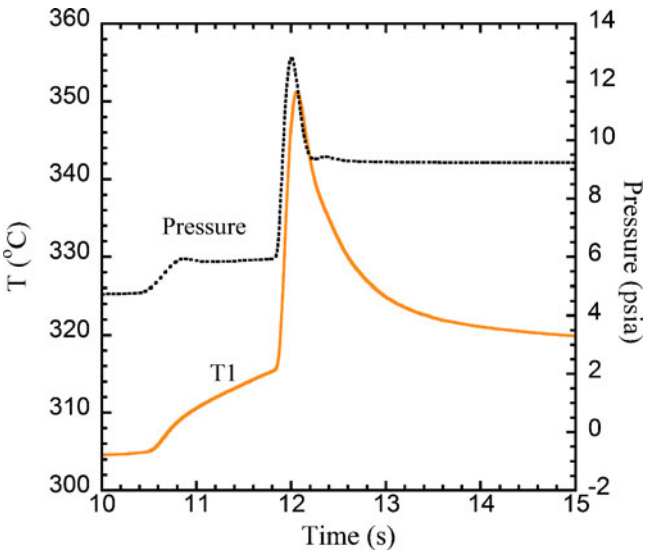

(d) $t = 10$ to 15 seconds of Fig. 2c

Fig. 2 Representative pressure and radial temperature histories associated with a **a** single cool flame, **b** cool flame followed by damped oscillation, and **c**, **d** two-stage ignition at reduced-gravity in a static, unstirred, spherical fused-silica reactor, i.d. = 10.2 cm, equimolar n-butane/oxygen premixture at $T_{\mathrm{initial}} = 304°\mathrm{C}$

In addition, prior to testing, the reactor was "aged" by running multiple tests and reproducibility of the data was confirmed. The internal reactor pressure was recorded at 100 Hz using a Setra 0-25 psia Model 204 transducer (accuracy: 0.028 psia = 1.4 Torr) located on the fill tube of the reactor. The radial gas temperature distribution was measured at five locations, starting at the center (T1) and every 1.3 cm from the center (i.e., thermocouple T2 was located at $\bar{R} = 1.3$ cm, T3 at $\bar{R} = 2.6$ cm, etc.) using type-K, 0.02 inch diameter, bare wire thermocouples mounted horizontally in the vessel through a common gas/thermocouple rake feedthrough. The temperature in the furnace was also measured with two type-K thermocouples, one of which provided feedback to a temperature controller used to maintain a uniform temperature within the furnace. Regarding testing, equimolar n-propane/oxygen and n-butane/oxygen premixtures were considered where the premixtures were prepared by partial pressure mixing and stored in a stainless-steel sample cylinder. A portion of the mixture was then transferred to a second, pre-evacuated sample cylinder. The reactor was then

evacuated to 20 mTorr (or less) at which time the vacuum pump was isolated and the gas sample was introduced into the vessel. Once the vessel was filled, the gas was allowed to equilibrate prior to the onset of a significant portion of the reaction for cases in which the chemical time was relatively long compared to the time required for establishment of the initial reactor conditions (quiescent flow, uniform initial temperature, prescribed initial reactant pressure).

Numerical Results and Discussion

Time-Dependent Temperature, Density and Species Concentration Profiles

From the numerical models, five representative cases were considered to illustrate the different reaction modes characteristic of low-temperature combustion. They include:

- Case 1: Weakly exothermic, slow reaction ($\bar{P}_o = 60$ kPa, $\bar{T}_o = 630$ K)
- Case 2: Strongly exothermic, slow reaction ($\bar{P}_o = 70$ kPa, $\bar{T}_o = 630$ K)
- Case 3: Damped oscillatory cool flame ($\bar{P}_o = 80$ kPa, $\bar{T}_o = 630$ K)
- Case 4: Damped oscillatory cool flame with large temperature excursion ($\bar{P}_o = 100$ kPa, $\bar{T}_o = 630$ K)
- Case 5: Two-stage ignition ($\bar{P}_o = 120$ kPa, $\bar{T}_o = 630$ K)

The non-dimensional temperature, θ; density, ρ; and reactant and intermediate, autocatalytic species concentrations, Y and X, histories at the center of the reactor are shown for each case in Figs. 3, 4, 5, 6 and 7. These plots include curves from both the compressible (Comp) and the Boussinesq (Bsq) models. In addition, Figs. 8 and 9 provide 2-D temperature contours with superimposed arrows indicating proportional velocities at various locations. (The fluid velocity at $R = 0$ for each case is given in the figure caption.) The times at which the profiles were taken coincide with the time for which the density difference between the models was the largest. For all slow reactions and cool flame cases (Cases 1–4), the computed density change was less than 10% and the Boussinesq approximation was adequate. With the Boussinesq approximation, density is solely a function of the temperature and included as a body force in the momentum equation, while the density in the compressible model is a variable determined by the equation of state (ideal gas law) for which the pressure and temperature are computed from

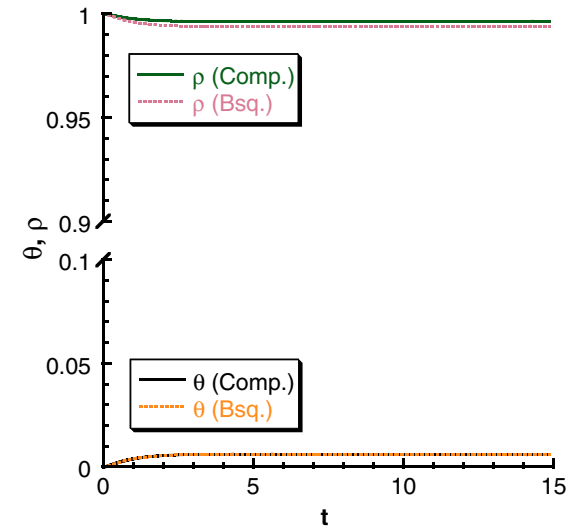

(a) $\theta(t, R = 0), \rho(t, R = 0)$

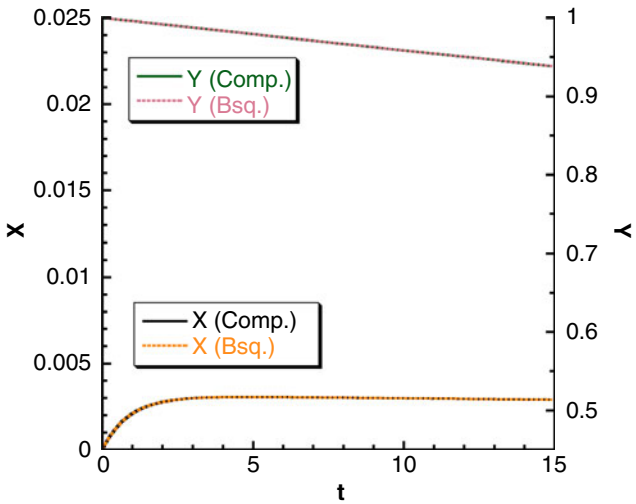

(b) $X(t, R = 0), Y(t, R = 0)$

Fig. 3 Plots of non-dimensional **a** temperature θ and density ρ and **b** lumped reactant concentration histories at the center of the reactor (mid-point of the axisymmetric axis) for a low-temperature reaction at $P_{\text{initial}} = 60$ kPa and $T_w = 630$ K

the coupled species conversation, momentum and energy equations listed above. As shown, the Boussinesq approximation did an excellent job at predicting flow properties and evolution of species for Cases 1–4 since the flows were solely buoyantly driven and the fluid temperature differences were small. For the multi-stage ignition case (Case 5), the change in density increases during the course of reaction (discussed below) and reaches 30–40% of its initial value prior to ignition. For this case, the Boussinesq assumption was valid in the early stages of reaction, yet not valid for later stages since $\Delta T / T_o << 1$ was not satisfied as the temperature increases (shown below in Fig. 7).

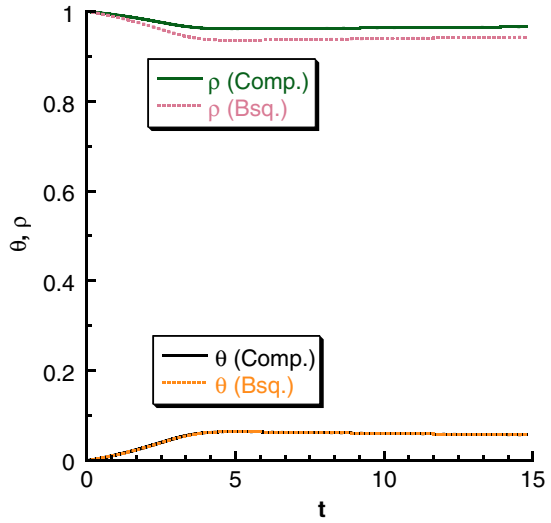

(a) $\theta(t, R = 0), \rho(t, R = 0)$

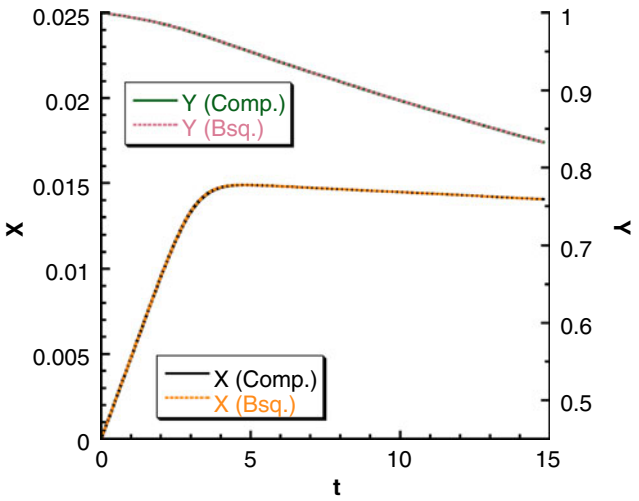

(b) $X(t, R = 0), Y(t, R = 0)$

Fig. 4 Plots of non-dimensional **a** temperature θ and density ρ and **b** lumped reactant concentration histories at the center of the reactor (mid-point of the axisymmetric axis) for a low-temperature reaction (with a higher initial temperature rise than Fig. 3) at $P_{\text{initial}} = 70$ kPa and $T_w = 630$ K

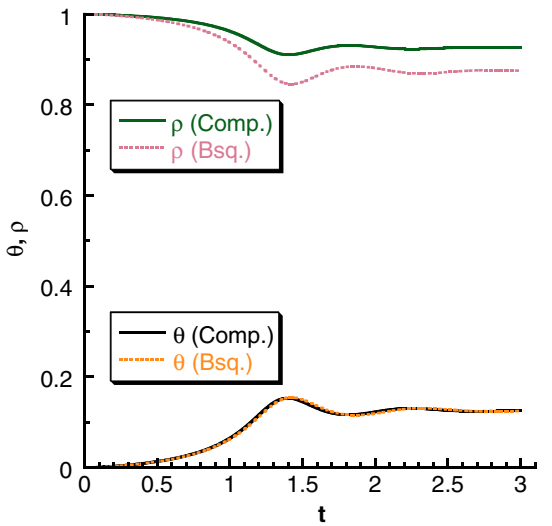

(a) $\theta(t, R = 0), \rho(t, R = 0)$

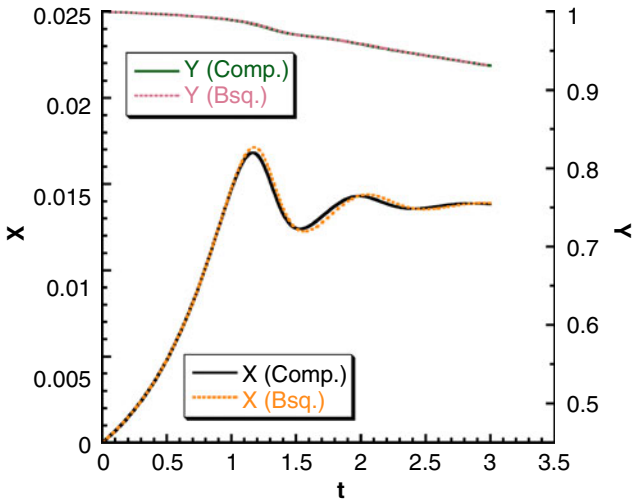

(b) $X(t, R = 0), Y(t, R = 0)$

Fig. 5 Plots of non-dimensional **a** temperature θ and density ρ and **b** lumped reactant concentration histories at the center of the reactor (mid-point of the axisymmetric axis) for a damped oscillatory cool flame at $P_{\text{initial}} = 80$ kPa and $T_w = 630$ K

Case 1 (Weakly Exothermic, Slow Reaction) For the weakest reaction considered (shown in Fig. 3), the temperature increased very slowly as a small fraction of the reactants were consumed. Here, the density change using either model was less than 1% such that the Boussinesq approximation was clearly satisfied as shown in Fig. 3a. Experimentally, slow reactions in unstirred reactors with similar transient behavior have been observed (Foster 2007).

The temperature and species concentration profiles for the two models are computationally the same. For this slow reaction, Fig. 3b shows that the reactants Y are continuously consumed, while the autocatalytic species X had an initial rapid increase, coinciding with the increase in temperature, and then slowly decreased as the reaction slowed.

Case 2 (Strongly Exothermic, Slow Reaction) For a case with a slightly higher initial pressure, a slow reaction characterized by a larger temperature excursion is shown in Fig. 4. Similar to the case shown in Fig. 3, the temperature increases in the early stage of the reaction and slowly decays over a longer time coincident with the decrease in the fuel concentration and autocatalytic species concentrations. In this case, the

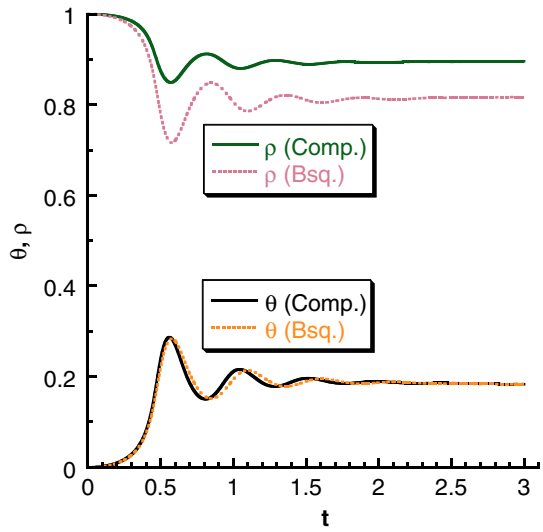

(a) $\theta(t, R = 0), \rho(t, R = 0)$

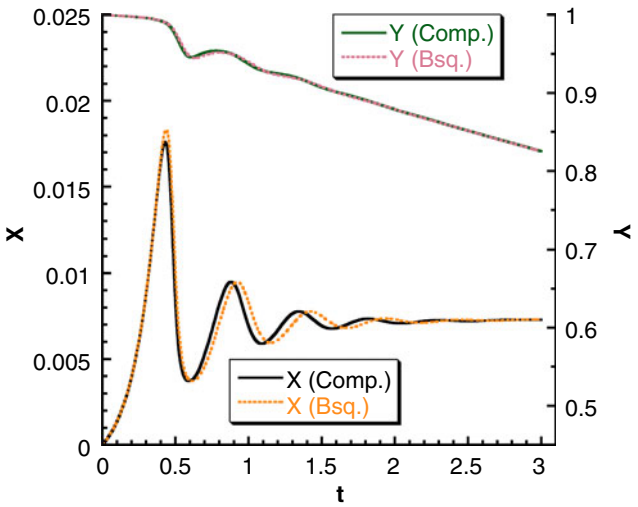

(b) $X(t, R = 0), Y(t, R = 0)$

Fig. 6 Plots of non-dimensional **a** temperature θ and density ρ and **b** lumped reactant concentration histories at the center of the reactor (mid-point of the axisymmetric axis) for a damped oscillatory cool flame at $P_{\text{initial}} = 100$ kPa and $T_w = 630$ K with a larger temperature rise than the case shown in Fig. 5

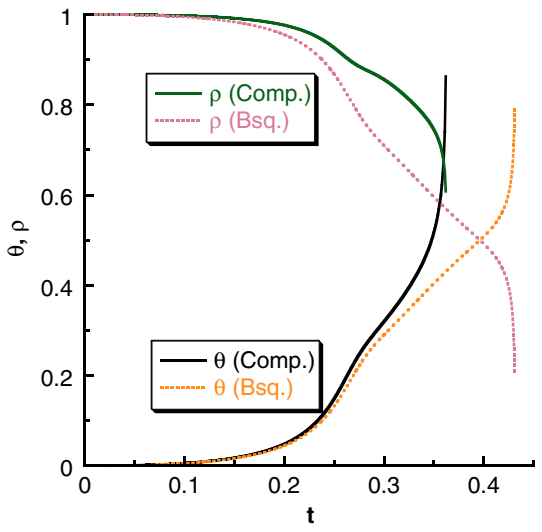

(a) $\theta(t, R = 0), \rho(t, R = 0)$

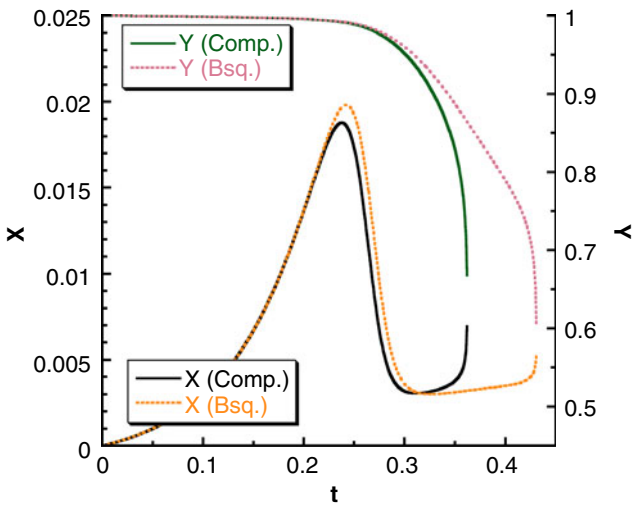

(b) $X(t, R = 0), Y(t, R = 0)$

Fig. 7 Plots of non-dimensional **a** temperature θ and density ρ and **b** lumped reactant concentration histories at the center of the reactor (mid-point of the axisymmetric axis) for a two-stage ignition at $P_{\text{initial}} = 120$ kPa and $T_w = 630$ K. Absolute tolerance for u and v was 10^{-3} for timely convergence

density change throughout the course of the reaction was at most 6%, such that the Boussinesq approximation was again sufficient as shown in comparison with the temperature and species concentrations (Fig. 4b) obtained using the compressible model and the simplified model. Overall, the trends associated with the slighly more exothermic Case 2 are similar to those shown in Case 1.

The peak non-dimensional temperature difference in both models was $\theta \approx 0.065$, which corresponds to $\Delta T = 41$ K at $T_w = 630$ K for the conditions considered herein. For this case, the temperature difference between the models was negligibly small (0.00025) at $t = 2.5$, a 0.625% difference. Even after the peak temperature, the difference between the models is negligibly small.

Case 3 (Damped Oscillatory Cool Flame) An oscillatory cool flame was predicted at a slightly higher initial pressure (as shown in Fig. 5). For this case, the peak temperature excursion was approximately 20% higher than the initial temperature. Not surprisingly, the density change was larger than that in either Cases 1 or 2, coincident with the increase in temperature at

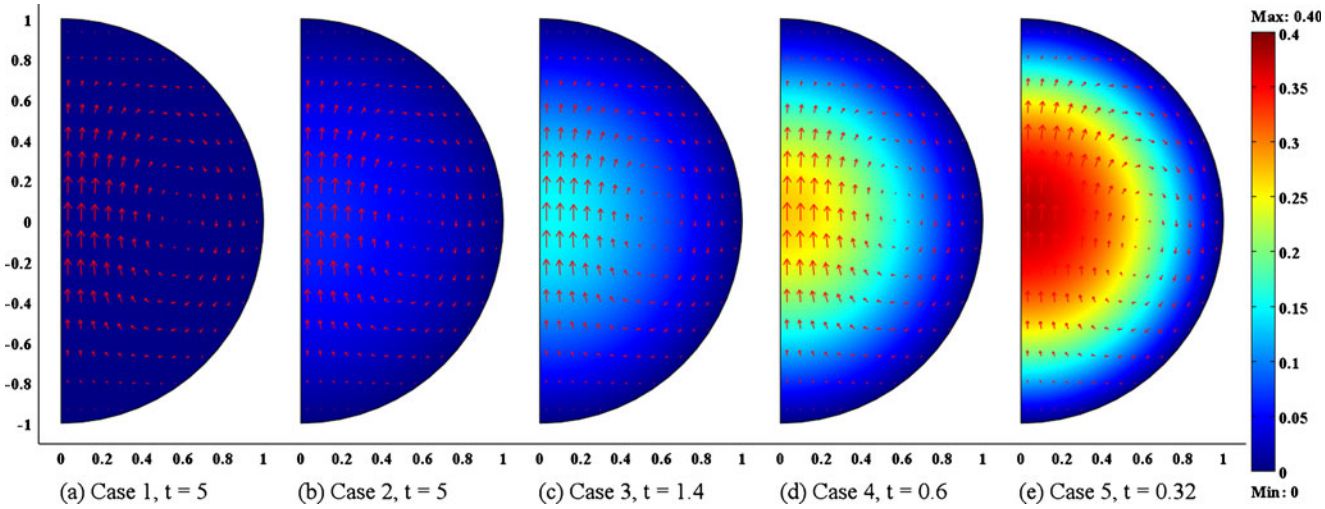

Fig. 8 Nondimensional temperature profiles with proportional arrows indicating the velocity field for each case described in Section "Numerical Results and Discussion" using the compressible flow model. V at R = 0 for each case is: **a** 0.011, **b** 0.15, **c** 0.45, **d** 1.23, and **e** 1.56

the center of the reactor, noting that the 2-D temperature and flow fields are shown in Figs. 8c and 9c for the two models. Specifically, the maximum density change at the center of the reactor (Fig. 5a) was 15% and 10% using the Boussinesq approximation and the compressible model, respectively. As expected, the Boussinesq model begins to break down for such cases in which the temperature rise is considerable. Again, however, the differences in the temperature and species concentrations are negligibly small. Interestingly, the compressible model did predict a very slight shift in the oscillation frequency (towards higher frequency), yet the difference decreased as the oscillations damp out. The temperature distribution shown in Fig. 2a for a representative cool flame test is qualitatively similar to that predicted computationally. Interestingly, the model captures the initial induction period followed by a significant temperature rise.

Case 4 (Damped Oscillatory Cool Flame with Large Temperature Excursion) An oscillatory cool flame with a larger initial temperature excursion is shown in Fig. 6 (with spatial profiles in Fig. 10) corresponding to a

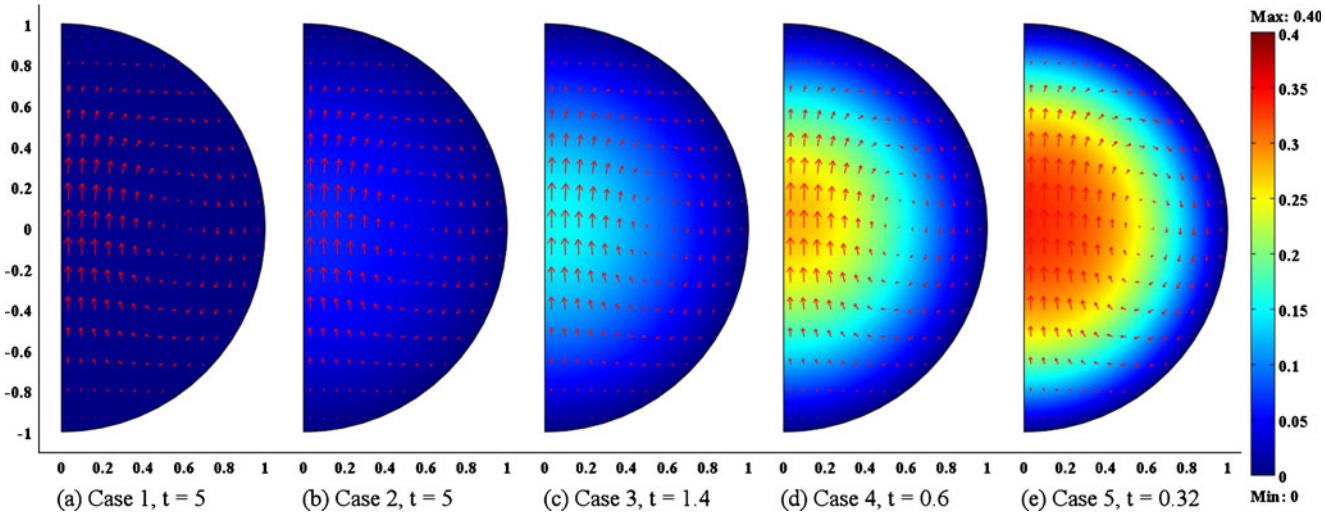

Fig. 9 Nondimensional temperature profiles with proportional arrows indicating the velocity field for each case described in Section "Numerical Results and Discussion" using the Boussinesq approximation model. V at R = 0 for each case is: **a** 0.011, **b** 0.15, **c** 0.49, **d** 1.42, and **e** 1.66

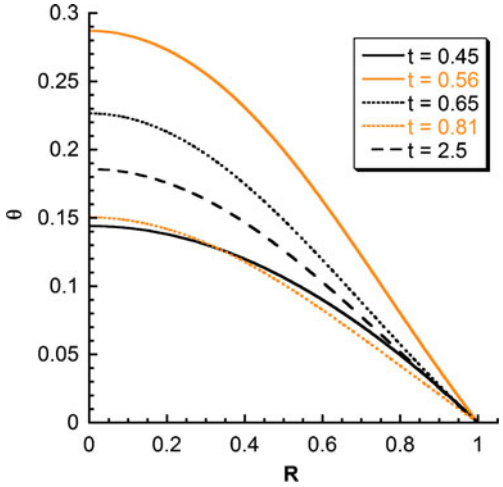

Fig. 10 Radial temperature profiles for Case 4, a damped oscillatory cool flame at $P_{\text{initial}} = 100$ kPa and $T_w = 630$ K

slightly higher initial pressure. For this case, the non-dimensional temperature has a maximum of approximately 0.29 ($\Delta T = 182.7$ K, for an initial temperature of 600 K), while the corresponding change in density exceeds 10%. As such, the Boussinesq approximation weakens and differences between the models begin to manifest themselves. Specifically, the compressible model shows that the oscillation frequency is slightly higher in the fully compressible case similar to Case 3. Both the models qualitatively capture the oscillatory nature of the empirical cool flames in Fig. 2b. It is also interesting to note that the reactant concentration Y at the center decreases as a function of time as shown in Fig. 6b, yet there is a small window of times near $t \approx 0.7$ in which the concentration of the parent mixture increases at the center following the initial temperature excursion. This increase indicates that the reactants that are depleted in the center are replenished from a higher concentration in the surrounding region. The recirculating velocity field, which is predicted by both models in Figs. 8d and 9d, may be responsible for transporting reactants to the depleted zone.

To visualize the increasing effect of natural convection on the recirculating pattern, Fig. 11 shows the temperature distributions at $t = 1.5$ for various values of $Ra/\bar{\beta}(\Delta\bar{T})$. Clearly, the maximum temperature shifts vertically upward along the symmetry axis with increasing $Ra/\bar{\beta}(\Delta\bar{T})$ as seen empirically.

Case 5 (Two-Stage Ignition) The models are also able to capture two-stage ignitions such as that shown in Fig. 7. As indicated, the models are in excellent agreement during the slow reaction period (accompanied by a small temperature increase), yet the models begin to substantially deviate from one another at $t \approx 0.275$ as the temperature excursion increases beyond $\theta \approx 0.30$ (i.e., the temperature at the center of the reactor is 30% higher than the initial/wall temperature). This trend compares qualitatively well with the experimental results shown in Fig. 2c and perhaps even more closely with results shown in Fig. 2d. The model based on

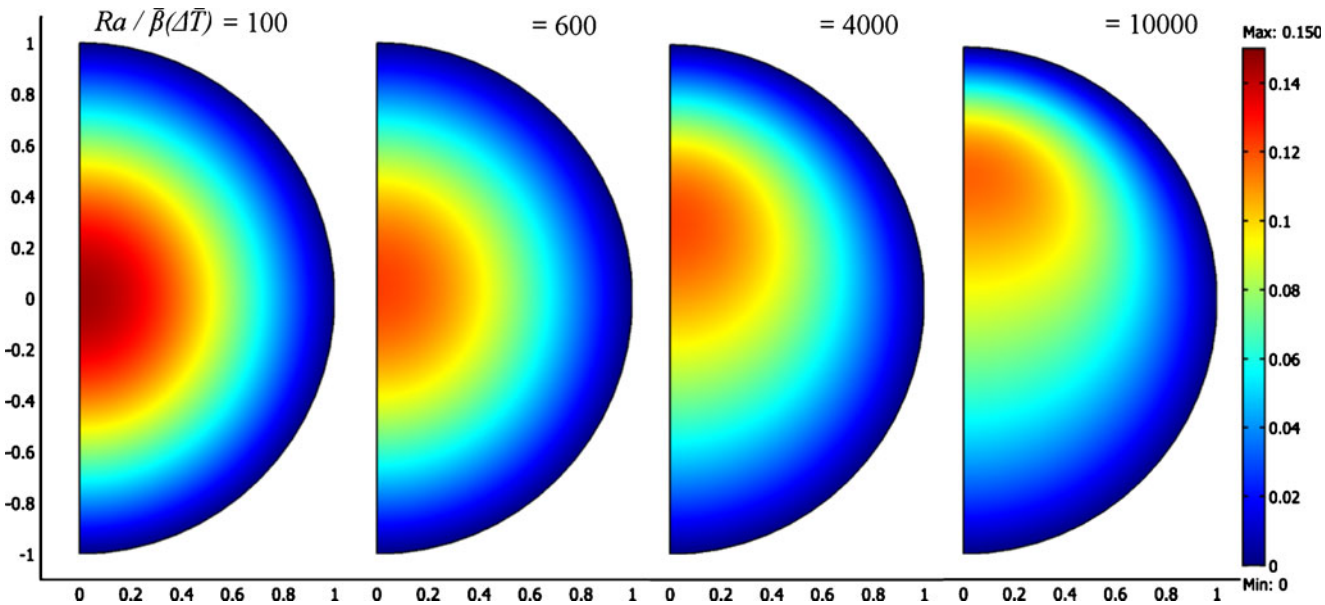

Fig. 11 Temperature profiles at times of peak temperature: $t = 1.8$ for $Ra/\bar{\beta}(\Delta\bar{T}) = 100$ and $t = 1.5$ for $Ra/\bar{\beta}(\Delta\bar{T}) = 600$, 4000, and 10000. These computations were performed using the compressible flow model

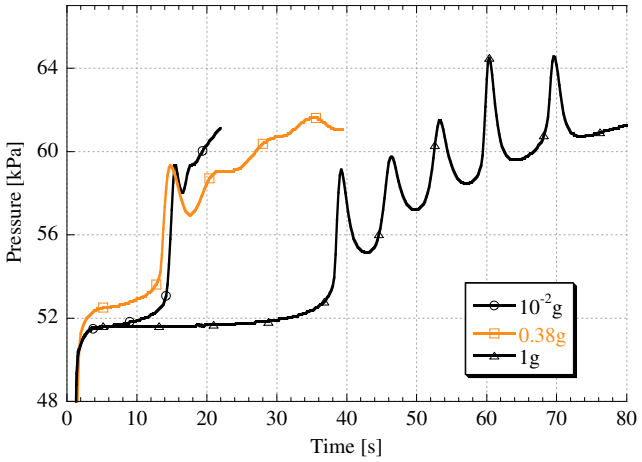

Fig. 12 Experimental pressure histories for equimolar propane/oxygen cool flames obtained at different gravity levels at a similar initial pressure showing that the induction time increases with increased stirring at 1g Foster (2006)

the Boussinesq approximation predicts a delay (nearly double) in the induction time ($\Delta t = 0.07$) prior to ignition. The delay may be attributed to the larger density difference computed for the Boussinesq model, which in turn intensifies the recirculation (in the captions for Figs. 8e and 9e, note the higher velocity indicated for the Boussinesq model) and promotes heat loss from the reactor. This result is qualitatively consistent with prior experimental observations (Foster and Pearlman 2006a; Foster 2006), which showed that increased stirring for low to moderate Rayleigh number flows (where Ra was varied by varying g) delays the onset of ignition through the increased heat transfer to the boundaries (see Fig. 12). This result is also consistent with the analytic and numerical predictions of Kagan et al. (1997) who also showed that short-scale stirring can delay thermal ignition limits.

Summary and Conclusion

Computations based on a compressible model were compared to those in which the Boussinesq approximation was used to assess the validity of the Boussinesq approximation for modeling low temperature combustion and multi-stage ignition. Clearly, damped oscillations can and do occur in low temperature hydrocarbon chemistry and the results acquired with the Wang–Mou model are qualitatively similar to those predicted by Fairlie et al.'s (2000) reduced chemistry mechanism and experimental results shown in Fig. 2 and reported by Pearlman (2007). As expected, for $\theta < 0.3$, the Boussinesq approximation is sufficient and differences in the computed non-dimensional temperature were shown to be less than 10% for the cases considered. For the multi-stage ignition case such as that shown in Fig. 7, the Boussinesq approximation is sufficient during early stages of the reaction in which the temperature excursion is relatively modest, yet it is not valid during the transition to ignition.

The effect of the non-dimensional group $Ra/\bar{\beta}(\Delta\bar{T})$ on the predicted temperature distribution was also considered. As $Ra/\bar{\beta}(\Delta\bar{T})$ increases, the peak temperature shifts vertically upward as observed in unstirred static experiments that have been previously reported in the literature. Notably, the values for $Ra/\bar{\beta}(\Delta\bar{T})$ used in the computational studies herein are consistent with published data showing that natural convection is important for $Ra \gtrsim 600$. As shown in Fig. 11, the non-dimensional peak temperature rise is approximately 0.15 and the onset of natural convection is evident at $Ra/\bar{\beta}(\Delta\bar{T}) = 4000$. Thus, the critical Ra for onset of convection based on this computational study is: $0.15 \cdot 4000 = 600$, which is consistent with prior experimental data (Tyler 1966; Fine et al. 1970).

Acknowledgements Special thanks are extended to Ming-Shin Wu, program administrator for NASA grant NCC3-1006; Rich Chapek for his support performing the experiments; and the NASA microgravity program for enabling the authors to perform the experiments aboard NASA's KC-135. The authors also acknowledge financial support for MF from the National Science Foundation Graduate Research Fellowship Program and George Fox University Grant GFU08G0007.

References

Barnard JA, Harwood BA (1974) Physical factors in the study of the spontaneous ignition of hydrocarbons in static systems. Combust Flame 22(1):35–42

Campbell AN, Cardoso SSS, Hayhurst AN (2005a) The influence of natural convection on the temporal development of the temperature and concentration fields for Sal'nikov's reaction, P→A→B, occurring batchwise in the gas phase in a closed vessel. Chem Eng Sci 60(21):5705–5717. doi:10.1016/j.ces.2005.04.062

Campbell AN, Cardoso SSS, Hayhurst AN (2005b) A scaling analysis of Sal'nikov's reaction, P→A→B, in the presence of natural convection and the diffusion of heat and matter. Proc R Soc, Ser A 461(2059):1999–2020

Campbell AN, Cardoso SSS, Hayhurst AN (2006) A scaling analysis of the effects of natural convection, when Sal'nikov's reaction: P→A→B occurs, together with diffusion and heat transfer in a batch reactor. Chem Eng Res Des 84(A7):553–561

Campbell AN, Cardoso SSS, Hayhurst AN (2007) A comparison of measured temperatures with those calculated numerically and analytically for an exothermic chemical reaction inside a

spherical batch reactor with natural convection. Chem Eng Sci 62(A7):3068–3082
Cardoso SSS, Kan PC, Savjani KK, Hayhurst AN, Griffiths JF (2004a) The computation of the velocity, concentration, and temperature fields during a gas-phase oscillatory reaction in a closed vessel with natural convection. Combust Flame 136(1–2):241–245
Cardoso SSS, Kan PC, Savjani KK, Hayhurst AN, Griffiths JF (2004b) The effect of natural convection on the gas-phase Sal'nikov reaction in a closed vessel. Phys Chem Chem Phys 6:1687–1696
COMSOL AB (2008) COMSOL Multiphysics reference guide, version 3.5a
Fairlie R, Griffiths JF, Pearlman H (2000) A numerical study of cool flame development under microgravity. Proc Combust Inst 28:1693–1699
Fairlie R, Griffiths JF, Hughes KJ, Pearlman H (2005) Cool flames in space: experimental and numerical studies of propane oxidation. Proc Combust Inst 30:1057–1064
Fine DH, Gray P, MacKinven R (1970) Thermal effects accompanying spontaneous ignitions in gases. II. The slow exothermic decomposition of diethyl peroxide. Proc R Soc London, Ser A 316(1525):241–254
Foster M (2006) Earth, partial, and reduced gravity experiments and numerical work on propane-oxygen cool flames at subatmospheric pressures. Master's thesis, Drexel University
Foster M (2007) Low-temperature reactions and cool flames in an unstirred, static reactor at terrestrial and reduced-gravity. PhD thesis, Drexel University
Foster M, Pearlman H (2006a) Cool flames at terrestrial, partial and near-zero gravity. Combust Flame 147(1–2):108–117
Foster M, Pearlman H (2006b) Diffusion-controlled cool flame propagation speeds. In: 44th AIAA aerospace sciences meeting and exhibit, AIAA-2006-1132
Foster M, Pearlman H (2007) Cool flame propagation speeds. Combust Sci Technol 179:13–49
Frank-Kamenetskii DA (1955) Diffusion and heat transfer in chemical kinetics. Princeton University Press, Princeton
Hindmarsh AC, Brown PN, Grant KE, Lee SL, Serban R, Shumaker DE, Woodward CS (2005) SUNDIALS: Suite of nonlinear and differential/algebraic equation solvers. ACM Trans Math Softw 31(3):363–396
Kagan L, Beresycki H, Joulin G, Sivashinsky G (1997) The effect of stirring on the limits of thermal explosion. Combust Theory Model 1(1):97–111
Liang C, Mou C, Lee D (2003) Dynamic behavior and sensitivity of skeleton thermokinetic model for acetaldehyde oxidation. Chem Eng Sci 58:4173–4184
Pearlman H (2000) Low-temperature oxidation reactions and cool flames at earth and reduced gravity. Combust Flame 121(1–2):390–393
Pearlman H (2007) Multiple cool flames in static, unstirred reactors under reduced-gravity and terrestrial conditions. Combust Flame 148:280–284
Pearlman H, Foster M (2008) The role of diffusive transport on low and intermediate temperature hydrocarbon oxidation: closed reactor experiments using equimolar n-C4H10+O2 premixtures at reduced-gravity. Combust Sci Technol 180(2):219–229
Pearlman H, Foster M, Karakacak D (2003) Cool flames in propane-oxygen premixtures at low and intermediate temperatures at reduced-gravity. In: Seventh international workshop on microgravity combustion and chemically reacting systems, pp 193–196
Semenov NN (1935) Chemical kinetics and chain reactions. Oxford University Press, Oxford
Tyler BJ (1966) An experimental investigation of conductive and convective heat transfer during exothermic gas phase reactions. Combust Flame 10(1):90–91
Wang X, Mou CY (1985) A thermokinetic model of complex oscillations in gaseous hydrocarbon oxidation. J Chem Phys 83(9):4554–4561